COMPARISON OF POWERED-LIFT TURBOFAN AIRCRAFT WITH CONVENTIONAL TURBOPROP AIRCRAFT FOR ESTOL APPLICATION

Corin Gologan, Dieter Schmitt
Bauhaus Luftfahrt

Keywords: *Aircraft Design, Powered Lift, ESTOL*

Abstract

The focus of this paper is on methods for field performance calculation of powered-lift internally blown flaps (IBF) turbofan aircraft and conventional turboprop aircraft. These methods are the basis for the sizing of extreme short take-off and landing (ESTOL) aircraft, and, hence, the basis for a comparison the overall mission performance. In an application example, turbofan aircraft with IBF and conventional turboprop aircraft are sized for field length requirements between 600 m and 1000 m. Their mission performance is compared to a conventional take-off and landing turbofan aircraft for a typical regional aircraft design mission.

1 Introduction

The ACARE agenda defines challenging goals for emissions and noise reductions as well as for the increase of transport capacity and reduction of delays [1]. Previous publications have discussed the potential of extreme short take-off and landing (ESTOL) regional jets to increase airport capacity [2], [3]. Unconventional approach trajectories that require low-speed operation have been investigated experimentally and theoretically at NASA and the German Aerospace Center (DLR) for airport noise reduction [4-8]. Studies on economic implications of ESTOL aircraft for capacity increase and delay reduction have discussed potentials for successful ESTOL aircraft introduction [9], [10].

In previous studies the authors have shown that turbofan aircraft with powered lift can only achieve ESTOL performance with a higher fuel burn compared to a conventional take-off and landing (CTOL) aircraft [11], [12]. Capacity increase through such aircraft is therefore conflicting with the goal of reducing emissions. Especially under consideration of the increasing importance of environmental requirements, conventional turboprop aircraft could be a more efficient alternative to achieve ESTOL performance: Existing conventional turboprop aircraft with mechanical high-lift devices have shorter field length performance than turbofan aircraft. Thus, the question arises, if sizing for ESTOL performance could be achieved without the use of powered-lift devices and with a lower fuel burn penalty than powered-lift aircraft.

Therefore the focus of this study is the comparison of conventional turboprop aircraft with mechanical high-lift devices with powered-lift turbofan aircraft (IBF is selected representatively for powered lift). The design mission investigated is a typical regional aircraft mission with 68 passengers and a design range of 1,000 nm. The field length requirements investigated range from 600 m to 1000 m.

The methods for the determination of the performance related to take-off and landing are integrated into a parametric aircraft model. With this model, CTOL reference aircraft are designed first. Based on these reference aircraft, aircraft with IBF and conventional turboprop aircraft are sized for different ESTOL requirements. Finally, their design mission fuel burn is compared to the CTOL reference aircraft.

2 Aircraft System Modeling

The performance requirements related to take-off and landing are the design drivers for ESTOL aircraft. Their determination is the focus of this chapter. Simple empirical methods for conventional turbofan aircraft are available

in numbers of handbooks. For turboprop aircraft in the investigated class an empiric approach has been developed by Scholz and Nița [13]. These empiric approaches do not apply to IBF aircraft due to the interaction of thrust and lift and, hence, cannot be used for a consistent comparison. The methods developed by the author for CTOL turbofan aircraft and turbofan aircraft blown flaps (incl. IBF) [14] are used. A summary of these methods is given in this chapter. The focus is on the application of these methods to conventional turboprop aircraft. By the use of the same methods for all aircraft types investigated, a consistent comparison is assured. These methods are used to adapt the parametric aircraft model of the commercial aircraft conceptual design tool Pacelab APD [15] for this specific application. The APD methods used are mainly methods of Torenbeek [16] and are only briefly addressed here.

2.1 Low-Speed Engine Performance

2.1.1 Turboprop

The low-speed turboprop engine performance model has to provide the thrust lapse during take-off, i.e. the engine thrust as a function of the Mach number. For turboprop engines the shaft power increases with increasing speed due to the increased dynamic pressure at the inlet. However, turboprop engines are generally flat rated to a certain maximum take-off power. Therefore, constant take-off power P_0 with increasing speed is assumed. The thrust lapse is then calculated for different speeds with:

$$T = P_0 \frac{\eta}{v} \qquad (1)$$

Thereby, a generic ideal propeller efficiency map based on reference [17] (cf. app. Fig. 11) is used to calculate the propeller efficiency η. This generic map is calibrated with a k-factor of 0.9 to provide more realistic values with a reference efficiency of η=0.78 in cruise condition.

For zero airspeed, equation (1) is not defined. Here, the sea level static thrust (SLST) T_0 is calculated with (cf. e.g. [18]):

$$T_0 = \left(\eta_0 \cdot P_0 \cdot \sqrt{2 \cdot \rho \cdot A}\right)^{\frac{2}{3}} \qquad (2)$$

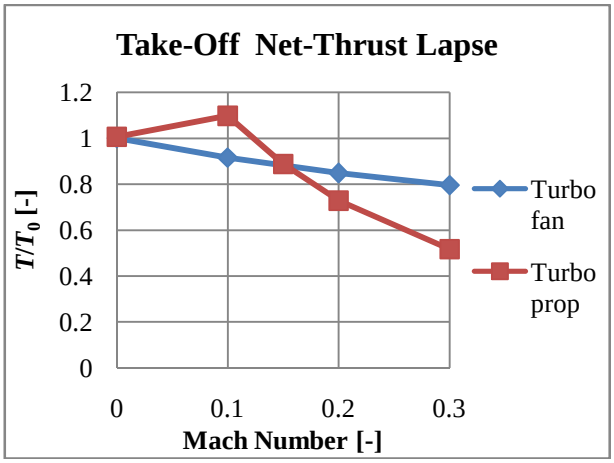

Fig. 1 Take-off net-thrust lapse

The propeller efficiency calculated from the efficiency map at Mach=0.1 is assumed for the static condition.

Fig. 1 shows the resulting thrust lapse for the turboprop and turbofan (cf. section 2.1.2) reference aircraft normalized by the SLST. For the turboprop engine, the thrust at Mach=0.1 is higher than the SLST, which results from the definition of the SLST in equation (2) and the usage of the same propeller efficiency. Important to note is that the thrust lapse for the turboprop engine given in Fig. 1 is plotted normalized by T_0 only for comparison reasons with the turbofan engine. A scaling of the thrust-lapse with T_0 would not represent the physical quality of a turboprop engine, as thrust scales linearly with P_0 (cf. equation (1)). T_0 scales with $P_0^{(2/3)}$ only (cf. equation (2)).

2.1.2 Turbofan

The low-speed engine model for the turbofan aircraft is based on a generic high bypass ratio separate flow turbofan engine modeled with the gas turbine simulation tool GasTurb [19] and documented in reference [14]. A bypass ratio of 5.0 is selected there for IBF to provide a sufficient fan pressure ratio of 2.0. A fan pressure ratio of around 2.0 is required to provide an exhaust Mach number of near 1.0 at the IBF ([20]). Parametric off-design studies with the reference engine are performed using the standard component maps of GasTurb to determine the low-speed engine characteristics. For the conventional turbofan aircraft the studies provide the net thrust as a function of the Mach number for sea level (cf. Fig. 1). As

expected, the turboprop engine has the higher thrust decrease with increasing Mach number.

For the IBF engine model, air offtake has to be considered. Fig. 2 shows a sketch of the offtake method considered for the IBF system. The entire bypass of the engine is taken off the engine and transmitted to the IBFs.

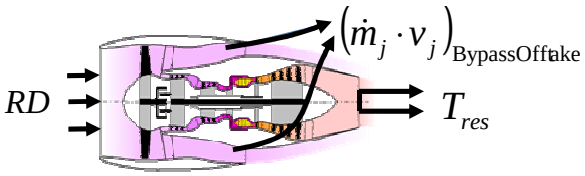

Fig. 2. Sketch of air offtake for IBF system (based on engine sketch of reference [19])

Required for the calculation of the aerodynamic characteristics of the IBF system is the jet momentum $\dot{m}_j \cdot v_j$ of the bypass offtake. For an ideal offtake without pressure losses, the bypass jet momentum is equivalent to the bypass gross thrust. The core thrust (T_{res}) acts conventionally in forward direction. Additionally, the ram drag (*RD*) has to be determined.

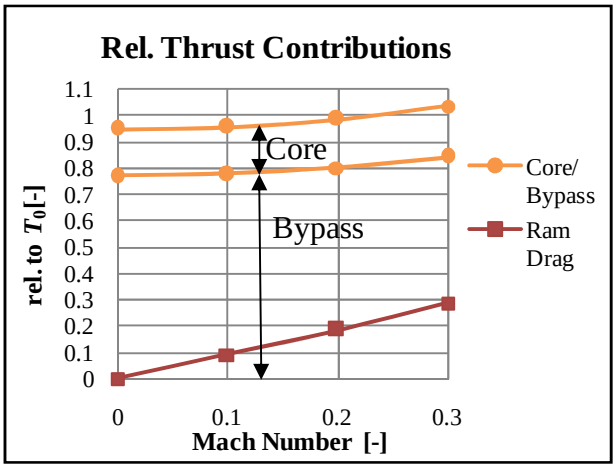

Fig. 3 Low-speed characteristics of turbofan engine with bypass offtake

Fig. 3 shows the bypass jet momentum and the residual gross thrust normalized by T_0 for different Mach numbers. Thereby, transmission duct pressure losses of 6% are assumed.[1] Due to the duct pressure losses, the sum of the core and bypass contribution at static condition is less than 1.0. Included also in Fig. 3 is the relative ram drag. The characteristics for the turbofan engine given in Fig. 1 and Fig. 3 are scaled with T_0.

[1] Different duct pressure losses were simulated (see ref [14]) to conduct sensitivity studies for this parameter.

2.2 Low-Speed Aerodynamics

2.2.1 Mechanical High-Lift Devices

The low-speed aerodynamic performance for the turboprop and turbofan aircraft with mechanical high-lift devices (single slotted fowler flaps) is calculated according to Torenbeek appendix G [16]. Drag increments due to flap extension and landing gear are added to the clean drag polar (section 2.6) and the maximum lift coefficients $C_{L\max}$ are calculated. Drag increment and $C_{L\max}$ are calculated as a function of flap angle, relative flap chord, spanwise flap extension and fuselage diameter.

2.2.2 Internally Blown Flaps

The low-speed aerodynamic performance of powered-lift aircraft cannot be modeled with standard methods due to the interaction of engine thrust and low speed aerodynamic performance. The aerodynamic coefficients for powered-lift aircraft are a function of the jet momentum coefficient, which is the ratio of the engine jet momentum to the dynamic pressure and the reference area:

$$C_\mu = \frac{\dot{m}_j \cdot v_j}{\frac{\rho}{2} \cdot v^2 \cdot S} \qquad (3)$$

For the investigated IBF system, the relevant jet momentum (bypass jet momentum) is calculated with the characteristics given in Fig. 3.

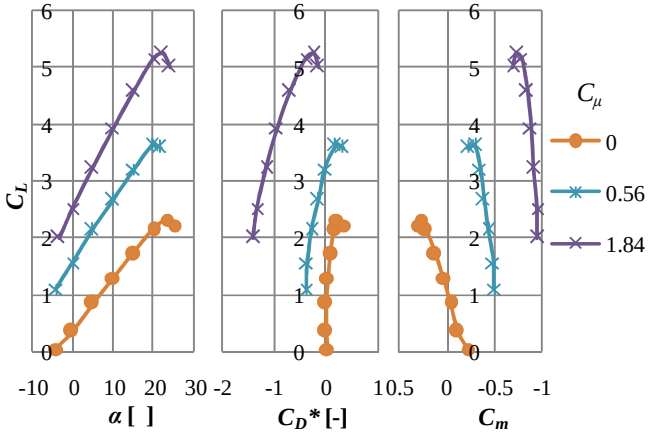

Fig. 4. Low-speed polar of IBF wind-tunnel model, δ_f=15°, (profile drag corrected)

Wind-tunnel experimental data of a NASA 3-D experiment [21] are used as a basis for the calculation of the low-speed aerodynamic performance of the IBF aircraft. Fig. 4 shows

the aerodynamic polars of the wind-tunnel model with the flaps in take-off configuration. One can see the dependency of lift coefficient, drag coefficient and pitching moment coefficient of C_μ. Consequently (cf. eq. (1)), the aerodynamic coefficients are a function of the engine jet momentum, (e.g. lift coefficient is increasing with increasing jet momentum), of the airspeed, or, of the reference area (e. g. for a given jet momentum the lift coefficient is decreasing with increasing airspeed or reference area). Drag coefficient can reach negative values as it includes the bypass jet momentum. These characteristics are important for the calculation of take-off and landing field length, as this means that the aerodynamic coefficients are changing during take-off and landing.

Lift, pitching moment, induced drag (including the forward contribution of the jet momentum) are calculated directly from the wind-tunnel polar. The profile drag is calculated according to section 2.2.1 to assure comparability of the IBF model and the model for the aircraft with mechanical high-lift devices.

2.2.3 Drag Due to Engine Failure

Drag due to engine failure is important for the calculation of the take-off field length, as it affects the lift-to-drag ratio during the one engine inoperative (OEI) take-off climb segment and during missed approach with OEI. The relevant contributions according to Torenbeek, app. G are the additional drag due to wind-milling engine, propeller drag, and drag due to asymmetric flight condition. Drag due to wind-milling engine and propeller drag are considered according to Torenbeek, app. G. The minimum drag due to asymmetric flight condition according to Torenbeek is found for a small sideslip angle. However, flight without sideslip causes only very little drag increment and simplifies the calculation of this additional drag: In this case the contribution of the vertical tail is most important (Torenbeek, app. G). For the aircraft with powered lift it is considered that the inoperative engine reduces the lift on the respective half-wing causing a rolling moment that has to be trimmed by the ailerons. Drag increment due to aileron deflection is modeled according to Roskam [22], p. 82.

2.3 Take-Off Field Length

For take-off field length calculation, the take-off speed has to be calculated first. For the turboprop aircraft and the conventional turbofan aircraft take-off speed is calculated in a standard way from the maximum lift coefficient for the respective flap setting (cf. section 2.2.1). For powered-lift aircraft the maximum lift coefficient is a function of the speed itself, which requires an iteration of the take-off speed. Engine failure causes a reduction of lift. The resulting implications related the determination of the take-off speed for powered-lift aircraft are documented in references [12] and [14].

For the calculation of the take-off field length empirical methods do not apply to powered-lift aircraft. Therefore, more detailed methods have been developed and documented in reference [14]. They consider the three cases according to FAR-25, from which the longest is the balanced field length (BFL):

1) Take-off with all engines operative (AEO): Acceleration with AEO, rotation, and climb to 35 ft plus a 15 % margin.
2) Take-off with one engine inoperative (OEI): Acceleration with AEO to decision speed v_1, acceleration to v_{TO} with OEI, rotation, and climb to 35 ft.
3) Acceleration with AEO to v_1, 2 seconds reaction time, and deceleration to full stop.

The ground roll distance is calculated numerically (cf. reference [14]):

$$\Delta x = \frac{m_{TO} \cdot v \cdot \Delta v}{T_{\text{res}} - RD - D_{\text{wm}} - q \cdot S \cdot C_D^* - \mu \cdot (m_{TO} \cdot g - q \cdot S \cdot C_L)} \quad (4)$$

The denominator represents the actual forces in x-direction, which during ground roll have to be calculated for zero angle of attack. T_{res} and RD are calculated from the low-speed engine model (section 2.1), C_D*, C_L from the low-speed polar (cf. section 2.2). Friction coefficient is assumed to be μ=0.03 during ground roll. Depending on the operating condition, AEO or OEI, the wind-milling drag D_{wm} of the engine and drag due to asymmetric flight condition (cf. section 2.2.3) are considered. The respective number of the operating engines is used for the calculation of the relevant thrust components.

The application of equation (4) to conventional turbofan and turboprop aircraft has the following implications: The residual gross thrust T_{res} is equivalent to the total gross thrust. The term (T_{res}-RD) is equivalent to the engine net thrust T and C_D* includes the aerodynamic drag only. Equation (4) then transforms into the numerical form of the analytical handbook formula (e.g. [23]) for ground roll calculation.

The distance required to climb to 35 ft clearance height (with AEO as well as OEI) and the related climb angle are calculated from the ratio of total force in x-direction to the lift. The total force in x-direction is calculated according to the denominator in equation (4) (for α at take-off) excluding the friction coefficient.

The breaking distance in case of aborted take-off is calculated with:

$$x_B = \frac{0.5 \cdot v_1^2}{\bar{a}} \qquad (5)$$

Typical average decelerations $\bar{a}$ are between 0.35g and 0.45g for turboprops and between 0.4g and 0.6g for jet aircraft [16]. For consistency reasons, a deceleration of 0.41g is used ($\bar{a}$ =4 m/s²) for all aircraft, for aborted take-off as well as for the deceleration segment for landing field length calculation.

Fig. 5 shows the BFL calculated with the above methods for turboprop aircraft over the take-off parameter according to Loftin's definition [24]:

$$TOP_{Prop} = \frac{(MTOW/S)\cdot(MTOW/P_0)}{\sigma} \qquad (6)$$

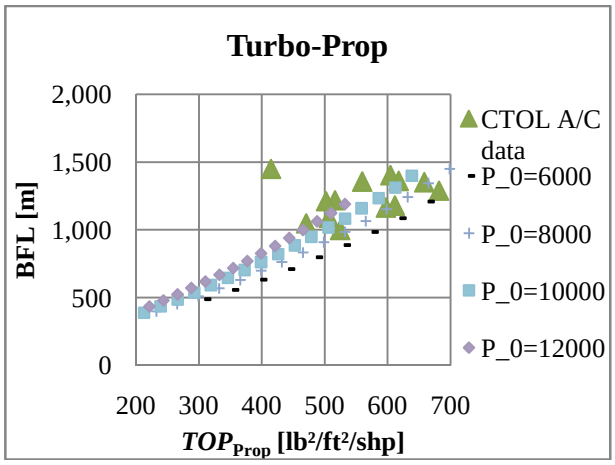

Fig. 5 Turboprop take-off performance

The dimensions of the turboprop reference aircraft (chapter 3) are used as a baseline. Wing-loadings between 175 kg/m² - 600 kg/m² and power loadings between 130 W/kg – 486 W/kg are applied for MTOW=23,000 kg. The flap setting is 15°, the spanwise flap extension is 75%, and the relative flap chord is 25 %. The resulting C_{Lmax} is between 2.5 and 2.65, depending on the wing loading[2]. The results show good agreement with existing turboprops. The variation of the results lies in the order of magnitude of the variation of the aircraft data.

Fig. 6 shows the BFL of 2-engine and 4-engine CTOL turbofan aircraft compared to 4-engine IBF aircraft over the take-off parameter for turbofan aircraft:

$$TOP_{Turbofan} = \frac{(MTOW/S)\cdot(MTOW/T_0)}{\sigma} \qquad (7)$$

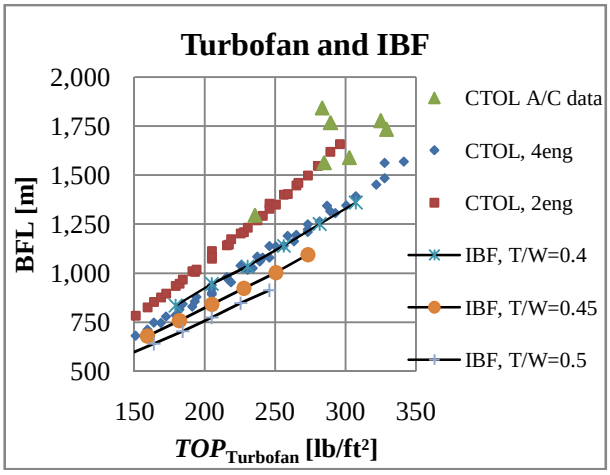

Fig. 6. Turbofan and IBF take-off performance

Similar flap design parameters are assumed for all turboprop and turbofan aircraft. Therefore, the definitions for the take-off parameters do not consider the take-off lift coefficient (as e.g. Loftin's definition does for turbofan aircraft).

For the turbofan aircraft, wing-loadings between 350 kg/m² and 600 kg/m² and thrust-to-weight ratios between 0.25 and 0.5 are applied for a MTOW of 24,000 kg. The maximum lift coefficient is between 2.28 and 2.35, depending on the wing loading. The 4-engine CTOL aircraft have shorter BFL for a given TOP compared to the 2-engine CTOL aircraft which

[2] For a constant relative spanwise flap extension, aspect ratio, taper ratio, and fuselage diameter C_{Lmax} increases with increasing wing area due to the increasing relative flapped area.

results from the better climb performance with OEI. The results for the 2-engine aircraft show good agreement with the CTOL A/C data that includes the 2-engine turbofan aircraft given in Tab. 7 of the appendix. The IBF aircraft have shorter BFL compared to the CTOL 4-engine aircraft only for thrust-to-weight ratios of more than around 0.4. Although the take-off speeds of the IBF aircraft are lower than for the CTOL aircraft, the BFL can be longer due to smaller climb angles with OEI. The smaller climb angles with OEI result from:

- duct pressure losses (here 6 %)
- loss in forward thrust due to the downward deflection of the bypass jet
- higher lift coefficients that result in higher induced drag

For this example, the lower take-off speed dominates the smaller climb angles with OEI only for thrust-to-weight ratios greater than 0.4.

2.4 Landing Field Length

For approach speed (v_{APP}) calculation, similar problems as for take-off speed calculation occur for the powered-lift aircraft due to the interdependence of thrust and low-speed aerodynamic performance. A combination of v_{APP} and thrust rating has to be found iteratively to meet the required safety margin to stall and the required approach angle. The low-speed engine model and the low-speed wind-tunnel data with the flaps in landing configuration are used for calculation of v_{APP}. For the algorithm implemented for the iteration of v_{APP} and thrust rating the authors refer to reference [14]. The newer FAR/EASA safety factor for v_{APP} ($1.23 \cdot v_{ST}$) is applied in this paper. Missed approach (MA) climb performance with AEO is calculated for v_{APP} and $C_{L,APP}$ with maximum available thrust and the flaps extended in final approach configuration. MA climb performance with OEI is calculated for the same flight condition with full OEI thrust and the flaps extended in MA with OEI configuration.

In empirical approaches, landing field length (LFL) is often calculated as a function of v_{APP}^2 (e.g. Loftin [24]). A more detailed approach is implemented here. Unfactored landing distance is the sum of different landing segments, i.e. approach distance from 50 ft, flare distance, and free roll (calculated according to Jenkinson [25]) and deceleration distance from touch-down speed to zero speed according to equation (5). An average deceleration of 4 m/s² is used. This method gives the possibility to study for example different approach angles. JAR-OPS 1.151 requires a safety factor of 1.67 for required LFL for turbofan aircraft and a safety factor of 1.43 for turboprop aircraft. This favors turboprop aircraft by around 17 % compared to turbofans with the same landing performance by definition [13].

Fig. 7 shows the LFL calculated for a -3° approach as a function of wing loading for the turboprop, turbofan and IBF (γ=-3° and γ=-6°) aircraft compared to data of existing turboprops and turbofan. The maximum lift coefficient for the turboprop aircraft is calculated according to section 2.2 for a flap setting of 30° and lies between 2.75 and 2.9, depending on the wing-loading. The turbofan aircraft have maximum lift coefficients between 2.55 and 2.9.

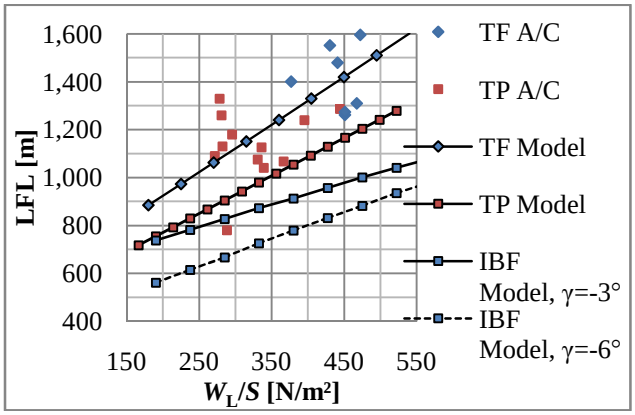

Fig. 7 Landing field length over wing-loading for investigated aircraft types

The aircraft data of the turboprop aircraft has a high variation, especially for lower wing loadings. Variations remain, even if the different flap designs are considered in the statistics (cf. [13]). This indicates high differences of the designs with respect to deceleration, and approach angles. The calculated trend for the -3° approach fits well with the data given for the ATR-72-500 and Bombardier Q-300 (cf. app. Fig. 13 for more detailed comparison with A/C data as well as trend for turboprops with γ=-6°). Important for the scope of this paper is a consistent calculation of the LFL with the same assumptions for all aircraft types. This is assured here by the application of the same methods, same flap characteristics (for

the conventional aircraft), and consistent values for deceleration and approach angles.

For the turbofan aircraft, the results of the implemented method are in the range of the aircraft data (cf. app. Fig. 14 for more detailed comparison with A/C data as well as trend for turbofan aircraft with γ=-6°). The lower calculated LFL of the conventional turboprop aircraft compared to the conventional turbofan aircraft is in the range of the difference that results from the different JAR requirements. The IBF aircraft have significantly lower LFL compared to the conventional turbofan aircraft, especially for the higher wing loadings. For the trend given in Fig. 7 (T/W=0.45, δ_f=55°), the maximum lift coefficient is between 5.2 (at W_L/S=180 kg/m²) and 5.68 (at W_L/S=540 kg/m²) resulting in approach speeds between 56 kts and 93 kts. With decreasing wing loading the difference between the conventional turbofan and the IBF aircraft decreases. The reasons are:

- decreasing jet momentum coefficient with increasing wing area, and, hence, decreasing $C_{L\max}$ of the IBF aircraft.
- increasing percentage of the approach and flare distance that is in the first order a function of the approach angle, which is the same for all aircraft.

For a required field length of 1,000 m, the required wing loading is 250 kg/m² for the conventional turbofan and 470 kg/m² for the IBF turbofan, which is a significant difference.

2.5 High-Speed Engine Performance and Engine Scaling

For the calculation of the mission performance the available thrust during climb and cruise condition as well as the specific fuel consumption are required. Engine dimensions are required for the calculation of the aerodynamic performance.

2.5.1 Turboprop

The turboprop engine performance model for high-speed (cruise and climb) is based on data given for the PW-120 in McCormick [26]. Included there is the take-off power $P_{0_{PW-120}}$, actual power P_{PW-120} and fuel flow FF_{PW-120} for climb as well as for cruise rating as a function of altitude and airspeed. For the purpose of this paper, these data are scaled with the required sea level engine shaft power for the respective rating.
The actual thrust is:

$$T = P\frac{\eta}{v} \tag{8}$$

Thereby, the propeller efficiency deck given in the appendix is used and adapted with a k-factor of 0.9 to provide more realistic values in cruise (cf. section 2.1.1).

Fuel flow of the PW-120 is normalized by the actual power of the PW-120 giving the actual power-specific fuel consumption (PSFC) for the different flight conditions. Thrust-specific fuel consumption (TSFC) is calculated from the power-specific fuel consumption:

$$TSFC = PSFC\frac{v}{\eta} \tag{9}$$

The engine nacelle scales according to Raymer [27] p. 251 as a function of engine power. The propeller diameter is kept constant, as the fuselage dimensions are kept constant and installation constraints have to be considered.

2.5.2 Turbofan

For the turbofan aircraft a generic turbofan engine with a bypass ratio of 5.0 documented in reference [14] is used. The data used here is the part load characteristic for SFC for the design altitude of 35,000 ft and the available climb and cruise thrust for different mach numbers. The engine deck is scaled with mass flow assuming constant specific thrust. Engine dimensions are calculated according to Jenkinson [25] and Raymer [27].

2.6 High-Speed Aerodynamics

The trimmed high-speed drag polar (clean configuration, no flaps, no gear) is calculated component-based according to Torenbeek [16], appendix F from the aircraft geometry. Thereby, lift-dependent profile drag of the components wing, fuselage, horizontal tail (HT), vertical tail (VT) and engines are calculated from the wetted areas. Wing wave drag is calculated as a function of sweep, airfoil type and airfoil relative thickness. Induced drag of wing, HT, and fuselage are considered.

2.7 Weights & Balance

OEW is calculated from the structural component weights, propulsion system weight, operational items weights, and equipment weight according to Torenbeek chapter 8. Landing gear weight is calculated according to Raymer [27]. Dry engine weight for the turbo-fan aircraft is calculated as a function of T_0, T_{SP}, *OPR* and *BPR* according to Torenbeek [16], Eq.4-36. Dry engine weight for the turbo-prop aircraft is calculated according to Raymer [27], as a function of the take-off power. The center of gravity (CG) is calculated component based with methods of Torenbeek [16], chapter 8. The wing is positioned such that the CG of the empty aircraft lies at 40 % of the mean aerodynamic chord. These component-based methods account for the scaling effects that occur due to the sizing of the main parameters *T/W* (*P/W* for turboprops) and *W/S* for the required performance and due to scaling effects over the entire mission. Weight penalties can be introduced for the different components, for example for penalties due to wing ducting or higher control surface weights.

2.8 Flight Performance

The mission simulation module of Pacelab APD [15] is used, which calculates numerically the mission performance (e.g. mission time and fuel burn) as well as point performance (e.g. climb performance at TOC) based on the aircraft drag polars, engine performance decks and weights.

3 Reference Aircraft

The design transport capacity is a payload of 68 passengers (6460 kg) over a design range of 1,000 nm. The fuel reserves are calculated based on a 200 nm alternate airport, 30 min loiter and a contingency of 5 % block fuel. The turbofan cruises at Mach 0.74 and 35,000 ft, the cruise condition for the turboprop is Mach 0.45 at 25,000 ft. The main lifting surface parameters of the reference aircraft (Tab. 1 and Tab. 2) are based on typical values given in Roskam part one [28]. Vertical tail (VT) volume coefficient is 0.09 and horizontal tail (HT) coefficient 1.0 for both aircraft. The fuselage size is based on existing aircraft with the same passenger capacity.

Parameter	Unit	Wing	VT	HT
AR	-	12	1.6	5
TR	-	0.6	0.6	0.6
φ_{25}	°	1.2	28	6

Tab. 1 Main lifting surface parameters of turboprop reference aircraft

Parameter	Unit	Wing	VT	HT
AR	-	8	1	5
TR	-	0.3	0.8	0.3
φ_{25}	°	20	40	28

Tab. 2 Main lifting surface parameters of turbofan reference aircraft

Trade studies are performed to determine the fuel burn optimized designs with respect to wing-loading and thrust-to-weight ratio (turbofan) respectively power-to-weight ratio (turboprop) considering a 300 ft/min climb constraint at top of climb. The resulting turbofan aircraft has a thrust-to-weight ratio of 0.29 and a wing-loading of 550 kg/m². This design has a BFL of 1,867 m and a LFL of 1,561 m for a -3° approach. The resulting turboprop aircraft has a power-to-weight ratio of 183 W/kg and a wing-loading of 375 kg/m². The BFL is 1,325 m and the LFL 1,017 m for this design. A value of 0.95 is assumed for both aircraft for the ratio of maximum landing weight (MLW) to MTOW, based on typical values of existing aircraft (cf. Fig. 12). The main design parameters and the resulting values for field length are in good accordance with existing conventional aircraft.

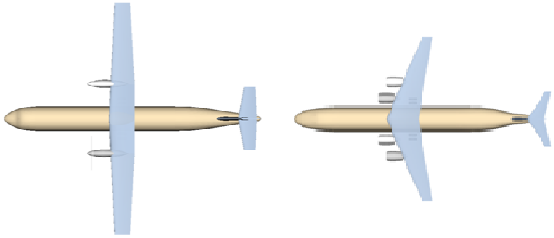

Fig. 8 Top-views of turboprop (left) and turbofan (right) reference aircraft

The conventional turboprop reference aircraft (cf. Fig. 8 for top-view) is the basis for the sizing of the turboprop aircraft for ESTOL performance. The conventional turbofan reference aircraft (cf. Fig. 8 for top-view) serves as a baseline for the IBF aircraft. A four-engine arrangement is selected, as engine failure is less critical for 4-engine IBF aircraft compared to a 2-engine arrangement.

For the investigated design mission, the turboprop has 3 % lower MTOW and 12 % less block fuel burn. The differences are due to 38 % lower SFC and 27 % higher lift-to-drag ratio. Lift-to-drag ratio is higher due to the higher aspect ratio and the flight condition near the maximum lift-to-drag ratio. Block time is 46 % longer for the turboprop aircraft.

4 Sizing for ESTOL Performance

The investigated aircraft that are sized for ESTOL performance are

- conventional turboprops based on the reference turboprop aircraft and
- powered-lift turbofan aircraft with IBF, based on the reference turbofan aircraft.

The IBF aircraft is modeled by the integration of the low-speed wind-tunnel polar and the low-speed engine model for IBF into the turbofan aircraft model.

The sizing for performance aims to find the best combination of the main design parameters ("design point")[3] that meets the required performance. The following performance requirements are considered:

- BFL and LFL required
- 2nd segment OEI climb rate required according to FAR/EASA
- MA climb rate required with OEI as well as with all engines operating (AEO) according to FAR/EASA
- the final approach angle required has to be maintained with OEI
- Climb rate required (300 ft/min) at top of climb (TOC)

For the determination of the design point, all combinations of the design parameters within a feasible design space are explored. For every combination, the performance for the above flight stages is calculated according to the methods given in chapter 2 and compared to the respective performance required. The resulting constraints are plotted in the matching chart, where the design point is selected.

Fig. 9 shows the matching chart of the IBF aircraft with a field length requirement of 1000 m. For this application a take-off flap angle of 15° gives the best trade-off between take-off speed and climb performance. The flap angle for final approach is 55° and for MA with OEI 45°[4]. The decisive constraints are the LFL required and the climb rate required for MA with OEI. The design point is W/S=500 kg/m² and T/W=0.44. The thrust-to-weight ratio required is significantly higher than the thrust-to-weight ratio required for the minimum climb rate at top of climb.

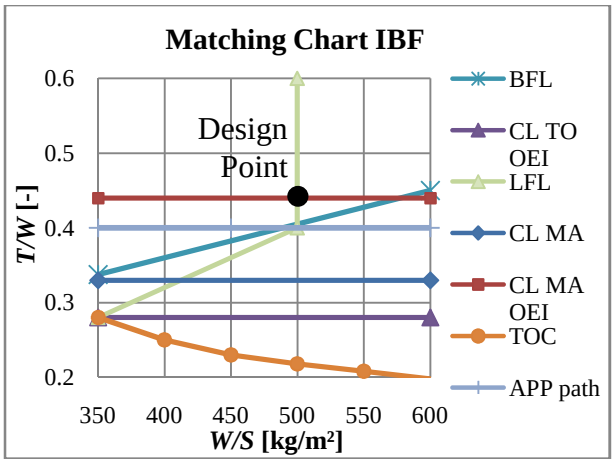

Fig. 9 Matching chart for aircraft with IBF sized for a 1000 m field length, -3° approach

All design points presented in the following were selected based on a matching chart. Here, it is discussed which of the constraints were the deciding ones. Tab. 3 shows the design points for the IBF aircraft with a -3° approach for different field length requirements. The wing-loading is always determined by the LFL required. T/W required is always determined by the MA with OEI, while T/W required to meet the BFL requirement is always lower. Consequently, the BFL is even below the BFL required.

		T/W [-]	W/S [kg/m²]
Field length [m]	1,000	0.44	500
	950	0.44	443
	900	0.44	385
	850	0.44	327

Tab. 3 Design points for different field length requirements, IBF aircraft with -3° approach

Tab. 4 shows the design points of the turboprop aircraft with the -3° approach for different field length requirements. For the 750 m and 800 m

[3] The main design parameters are W/S and T/W for the turbofan and W/S and P/W for the turboprop aircraft

[4] The determination of the optimum flap angles for final approach and missed approach with OEI is a complex task that is discussed in detail in reference [14]

requirement, the LFL determines *W/S*, while the climb rate required at TOC determines *P/W*. The BFL requirement is not a decisive constraint. For the 900 m field length requirement the LFL and BFL constraints determine the design point. For the 1000 m field length requirement, the design point selected represents the best compromise along the BFL-constraint with respect to mission fuel burn. The LFL requirement would allow for a higher wing loading (368 kg/m² for 1000 m LFL), but this would increase *P/W* to achieve the BFL required, and, hence, the mission fuel burn.

		P/W [W/kg]	*W/S* [kg/m²]
Field length [m]	1,000	190	330
	900	186	298
	800	196	230
	750	215	200

Tab. 4 Design points for different field length requirements, turboprop aircraft with -3° approach

Additionally, aircraft with a -6° approach angle were designed. The -6° approach reduces the LFL to 859 m for the turboprop and 1414 m for the turbofan reference aircraft.

Tab. 5 shows the resulting design points for the IBF aircraft. *T/W* is determined by the MA with OEI for all field length requirements. For the field length requirements ranging from 650 m to 800 m *W/S* is determined by the LFL required, BFL required is not decisive. For the field length requirements of 900 m and 1,000 m, the combinations of *T/W* and *W/S* along the BFL constraint that result in the minimum fuel burn are selected. A higher value for *W/S* could be selected, but would require higher *T/W* to meet the BFL constraint, and, thus have a higher block fuel.

		T/W [-]	*W/S* [kg/m²]
Field length [m]	1000	0.43	550
	900	0.43	485
	800	0.43	420
	700	0.43	325
	650	0.44	280

Tab. 5 Design points for different field length requirements, IBF aircraft with -6° approach

Tab. 6 shows the design points for the ESTOL turboprop aircraft with the -6° approach. Wing-loading is higher for the same field length requirement compared to the -3° approach aircraft due to the better landing performance. For the 600 m and 700 m field length requirement, *W/S* is determined by the LFL requirement, while at the same time the BFL requirement determines *P/W*. Including and above the 800 m field length requirement, the design points represent the best compromise along the BFL-constraint with respect to block fuel. The LFL requirement would allow for higher wing loadings (e.g. 463 kg/m² for the 1000 m field length requirement), but this would increase *P/W* to achieve the BFL required, and, hence, the block fuel.

		P/W [W/kg]	*W/S* [kg/m²]
Field length [m]	1000	190	330
	900	212	330
	800	223	310
	700	229	280
	600	205	215

Tab. 6 Design points for different field length requirements, turboprop aircraft with -6° approach

5 Field Length vs. Fuel Burn

Fig. 10 shows the design mission block fuel of the ESTOL aircraft relative to the fuel burn of the conventional reference turbofan aircraft for different field length requirements. Included are the trends for aircraft sized for a -3° approach and for a -6° approach. Considered is the sizing of the HT to provide a 10 % longitudinal static stability and the lift coefficient required for longitudinal trim. The VT is sized to trim the aircraft laterally in the case of OEI. For the tail sizing approach the author refers to reference [14].

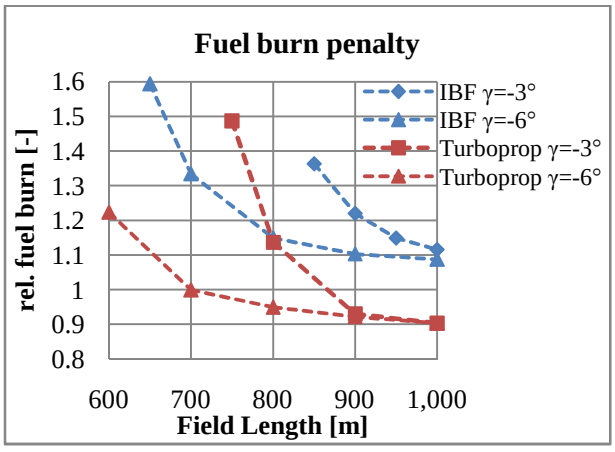

Fig. 10 Block fuel vs. field length[5]

[5] Field performance of reference aircraft:
Turboprop: BFL=1,325 m, LFL=1,017 m (859 m γ=-6°)
Turbofan: BFL= 1,867 m, LFL=1,561 m (1414 m, γ=-6°)

For a 1000 m field length requirement, the IBF aircraft have a fuel burn penalty of around 10 %, while the conventional turboprop has around 10 % less fuel burn. The fuel burn penalty increases reciprocally with decreasing field length due to scaling effects. For field lengths below 1000 m, the aircraft sized for the -3° approach have significantly higher fuel burn compared to the aircraft sized for the -6° approach. Thereby, the difference increases with decreasing field length. The IBF aircraft with the -3° approach has a fuel burn penalty of 36 % for a field length requirement of 850 m, while the turboprop achieves around 770 m with a similar fuel burn penalty. With a 20 % fuel burn penalty, the -6° aircraft achieve significantly lower field length (around 780 m for IBF and around 600 m for the turboprop) compared with the reference aircraft.

At the same fuel burn as the reference aircraft, the turboprop with the -6° approach achieves a field length of around 700 m, while the conventional turbofan has a BFL of 1,867 m and a LFL of 1414 m, which is a significant difference. The IBF aircraft with the -6° approach suffers from a fuel burn penalty of around 33 % to achieve the 700 m field length requirement. Important to note is that the values for the IBF aircraft represent a lower boundary for the fuel burn as potential weight and drag penalties due to IBF installation are not considered here.

The reason for the high differences between the aircraft designed for γ=-3° and γ=-6° is the significant contribution of the approach segment to the total LFL. The approach segment can only be reduced by reduced approach angle and not by reduced approach speed (respectively wing loading). Consequently, if very short field length is required, a steeper approach angle is a very efficient method for LFL reduction.

The lower design Mach number of the turboprop is the main reason for the better fuel burn characteristic compared to the IBF aircraft. Due to the lower design Mach number the turboprop has lower optimum wing-loadings for cruise condition. The lower wing-loadings improve the field performance, yielding in synergistic effects for ESTOL application. Consequently, ESTOL performance can be achieved with conventional mechanical flaps by increasing engine power and wing area with lower fuel burn penalties than for the powered-lift aircraft with IBF. However, the drawback of the turboprop aircraft (besides well known disadvantages like higher cabin noise, lower riding qualities etc.) is the longer block time (here 46 %) due to the lower cruise Mach number.

Conclusion and Outlook

Methods for the calculation and consistent comparison of field performance of

- turboprop and turbofan aircraft with mechanical high-lift devices
- turbofan aircraft with internally blown flaps (IBF)

have been developed, documented and compared to existing aircraft data. Conventional take-off and landing reference aircraft with turboprop and turbofan engines have been designed. Based on these aircraft, turboprop aircraft with mechanical high-lift devices and IBF turbofan aircraft have been sized for extreme short take-off and landing (ESTOL) requirements between 600 m and 1000 m. Thereby final approach angles of -3° and -6° have been considered.

The mission simulation results show that the aircraft with the -6° approach can achieve significantly shorter field lengths compared to the -3° approach aircraft for the same mission fuel burn. With a -6° approach, the turboprop aircraft have significantly reduced field length requirements at the same design mission fuel burn as the conventional reference turbofan aircraft. At the same time, the IBF aircraft has significantly higher fuel burn for the same field performance compared to the turboprop aircraft. For the investigated design mission the turboprop aircraft are a more fuel-efficient way to achieve ESTOL performance compared to the turbofan aircraft with IBF. Another advantage is the lower complexity due to conventional technologies (mechanical high-lift devices), while the disadvantage (from the mission performance point of view) is longer block time.

In the future, these studies can be extended by the investigation of different design Mach numbers for the turboprop aircraft to show a trade-off between fuel burn, field length, and block time.

Acknowledgments

The authors would like to thank Prof. Dr. Mirko Hornung, Hans-Jörg Steiner, Arne Seitz and Oliver Schmitz for valuable feedback and fruitful discussions.

Nomenclature

$\bar{a}$	Average deceleration
AR	Aspect ratio
A	Propeller area
BPR	Bypass ratio
C_D	Drag coefficient
C_D*	Equivalent drag coefficient (includes engine jet momentum
C_L	Lift coefficient
$C_{L,APP}$	Lift coefficient
C_m	Pitching moment coefficient
C_μ	Jet momentum coefficient
D_{wm}	Wind-milling drag
m_{TO}	Take-off mass
$\dot{m}_j$	Mass flow of IBF jet exhaust
OPR	Overall pressure ratio
P	Actual power
P_0	Sea level static power
$PSFC$	Power-specific fuel consumption
RD	Ram drag
S	Reference area
T	Actual net thrust
T_{res}	Residual thrust
T_0	Sea level static thrust
TOP	Take-off parameter
TR	Taper ratio
$TSFC$	Thrust-specific fuel consumption
TSP	Specific thrust
Δv	Speed increment
v	Airspeed
v_{APP}	Approach speed
v_1	Decision speed for aborted take-off
v_j	Velocity of jet exhaust
x_B	Breaking distance
α	Angle of attack
γ	Final approach angle
δ_f	Flap extension angle
η	Propeller efficiency
η_0	Propeller static efficiency
μ	Runway friction coefficient
ρ	Air density
σ	Density ratio relative to sea level
φ_{25}	Quarter-cord sweep

Abbreviations

BLF	Balanced field length
CL TO OEI	2nd segment climb rate with OEI
CL MA	Climb rate during missed approach
CL MA OEI	Climb rate during missed approach with OEI
IBF	Internally blown flaps
LFL	Landing field length
P/W	Ratio of sea level static power to MTOW
T/W	Ratio of SLST to MTOW
TF	Turbofan
TP	Turboprop
TOC	Top of climb
W/S	Wing loading (based on MTOW)
W_L/S	Wing loading (based on MLW)

References

[1] "Strategic Research Agenda - Volume 1" Advisory Council for Aeronautics Research in Europe. 2002

[2] Couluris, G.J., Hange, C.E., Wardwell, D.A., Signor, D. and Phillips, J. "A Potential Impact Analysis of ESTOL Aircraft on Newark Airport Operations," *AIAA Modeling and Simulation Technologies Conference and Exhibit*. Hilton Head, South Carolina. AIAA 2007-6700, 2007.

[3] Böck and Kelders, C. "Simulation of the Theoretical Capacity Potential of ESTOL Operations on an Intersecting Runway at Hub Airports," *9th AIAA Aviation Technology, Integration, and Operations Conference (ATIO)*. Hilton Head, South Carolina. AIAA 2009-6988, 2009.

[4] Hange, C. "Trajectory Kinematics of a Simultaneous Non-Interfering Landing Approach, and the Impact on ESTOL Regional Transport Performance and Flight Control," *3rd Annual Aviation Technology, Integration, and Operations (ATIO) Forum*. Denver, Colorado. AIAA 2003-6857, 2003.

[5] Hange, C. and Eckenrod, D. "Assessment of a C-17 Flight Test of an ESTOL Transport Landing Approach for Operational Viability, Pilot Perceptions and Workload, and Passenger Ride Acceptance," *45th AIAA Aerospace Sciences Meeting and Exhibit*. Reno, Nevada. AIAA-2007-1398, 2007.

[6] Bertsch, L., Looye, G., Otten, T. and Lummer, M. "Integration and Application of a Tool Chain for Environmental Analysis of Aircraft Flight Trajectories," *9th AIAA Aviation Technology, Integration, and Operations Conference (ATIO)*. Hilton Head, South Carolina. AIAA 2009-6954, 2009.

[7] Bertsch, L., Looye, G., Anton, E. and Schwanke, S. "Flyover noise measurements of a spiraling noise abatement approach procedure," *48th AIAA Aerospace Sciences Meeting Including the New Horizons Forum and*

Aerospace Exposition. Orlando, Florida. AIAA 2010-11, 2010.
[8] Bertsch, L., Schneider, O., Hemmer, H., Hepperle, M. and Macke, O. "Process Implementation for the System Evaluation of new Low-Noise STOL Transportation Concepts," *CEAS / KATnet II Conference on Key Aerodynamic Technologies*. Bremen, Germany. 2009.
[9] Peperak, M. "Economic Impact of the Hybrid Wing Cruise Efficient Short Take-Off and Landing (CESTOL) Commercial Aircraft," *International Powered Lift Conference 2008*. London, UK. 2008.
[10] Gologan, C., Kelders, C., Kuhlmann, A. and Seifert, J. Extreme Short Take-Off and Landing Regional Jets – Economic Motivation and Technological Challenges. *The Aeronautical Journal*, 2009, **113**(1147), 563-574.
[11] Gologan, C., Stagliano, F. and Seifert, J. "Vergleich von kurzstartfähigen Regionalflugzeugen mit aktiven Hochauftriebssystemen," *Deutscher Luft- und Raumfahrt Kongress*. Aachen. 2009.
[12] Gologan, C., Stagliano, S. and Schmitt, D. "Impact of ESTOL Capability on the Mission Fuel Burn of Regional Jets," *9th AIAA Aviation Technology, Integration, and Operations Conference (ATIO)*. Hilton Head, South Carolina. AIAA 2009-7096, 2009.
[13] Scholz, D. and Nita, M. Preliminary Sizing of Large Propeller Driven Aeroplanes. *Czech Aerospace Proceedings*, 2009, **2**, 41-47.
[14] Gologan, C. "A Method for the Comparison of Transport Aircraft with Blown Flaps," Dissertation. Institute of Leightweight Structures, Technical University of Munich. 2010.
[15] PACE. Pacelab APD. 2007.
[16] Torenbeek, E. *Synthesis of Subsonic Airplane Design*. (Delft University Press, Delft, 1982).
[17] Scholz, D. "Lecture Notes: Generic Engine Performance" Hamburg University of Applied Sciences, Department of Automotive and Aeronautical Engineering. 2000
[18] McCormick, B.W. *Aerodynamics of V/STOL Flight*. New York, London, 1967).
[19] Kurzke, J. GasTurb - Gas Turbine Performance Program. Dachau, 2007.
[20] Ball, T., Turner, S. and Marshall, D.D. "Short Takeoff Performance using Circulation Control," *46th AIAA Aerospace Sciences Meeting and Exhibit*. Reno, Nevada. AIAA 2008-174, 2008.
[21] Vogler, R.D. "Wind-Tunnel Investigation of Internally Blown Jet-Flap STOL Airplane Model" NASA TN D-8309. NASA Langley Research Center. 1976
[22] Roskam, J. *Airplane Design Part VI*. Ottawa, Kansas, 1985).
[23] Brandt, S.A. *Intorduction to aeronautics: a design perspective*. (AIAA, Blacksburg (Virginia, USA), 2004).
[24] Loftin, L.K. "Subsonic Aircraft: Evolution and the Matching of Size to Performance" NASA Reference Publication 1060. NASA Langley Research Center. 1980
[25] Jenkinson, L., Simpkin, P. and Rhodes, D. *Civil Jet Aircraft Design*. (Butterworth-Heinemann Ltd., Oxford, 1999).
[26] McCormick, B.W. *Aerodynamics, Aeronautics, and Flight Mechanics*. (John Wiley & Sons, Inc., Hoboken, NJ, 1995).
[27] Raymer, D.P. *Aircraft Design: A Conceptual Approach*. (AIAA, Reston, Virginia, 2006).
[28] Roskam, J. *Airplane Design Part I*. Ottawa, Kansas, 1985).
[29] Jane's. *Jane's All The World Aircraft 2000-2001*. (Jane's Information Group Inc., Coulsdon, Surrey, 2000).

Copyright Statement

Appendix

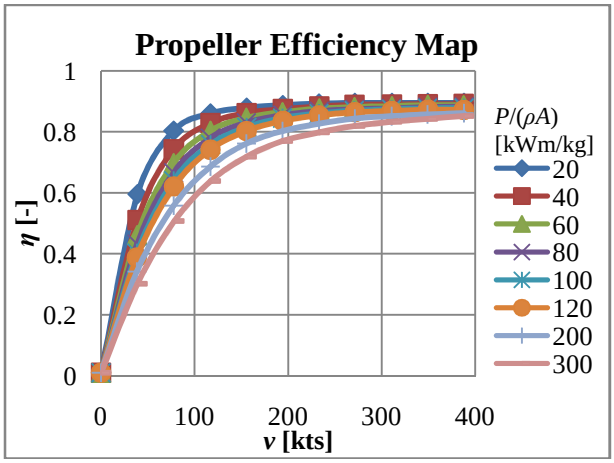

Fig. 11 Generic propeller efficiency map based on reference [17]

Turbofan	Turboprop
Bombardier CRJ 200	ATR-42-500
Bombardier CRJ 700	ATR-72-500
Bombardier CRJ 900	Bombardier Q-200-400
Embraer ERJ 145	Saab 340 and 2000
Embraer E170 (AR)	Antonov AN-140
Embraer E170 (LR)	Embraer 120
Embraer E175 (LR)	Fokker F-50
Avro RJ-70	IL-114-100
Fokker F-70	Dornier Do-328

Tab. 7 Aircraft included in statistics; Data collected from manufacturers' websites and reference [29]

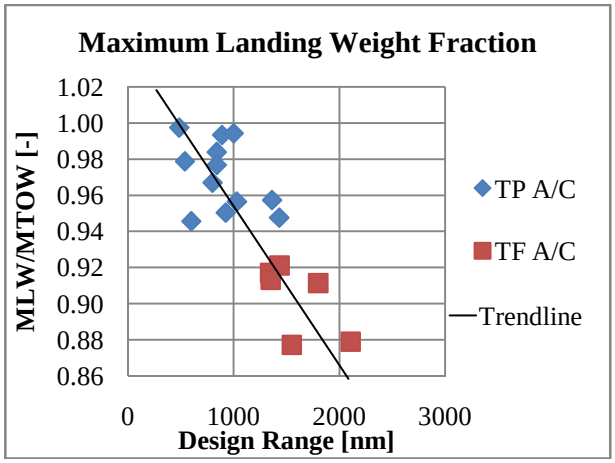

Fig. 12 Statistical data for determination of MLW-fraction

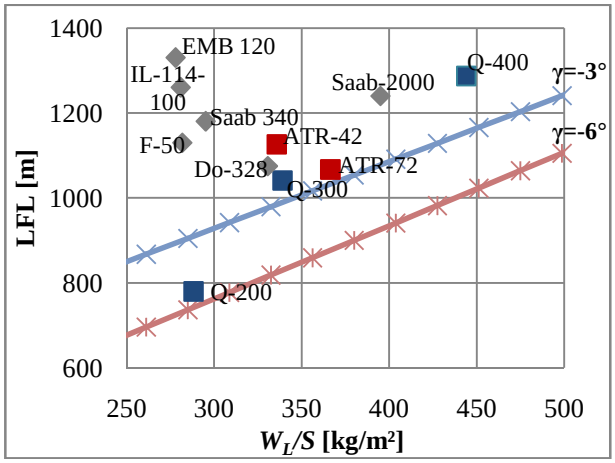

Fig. 13 LFL-method for turboprop compared to aircraft data

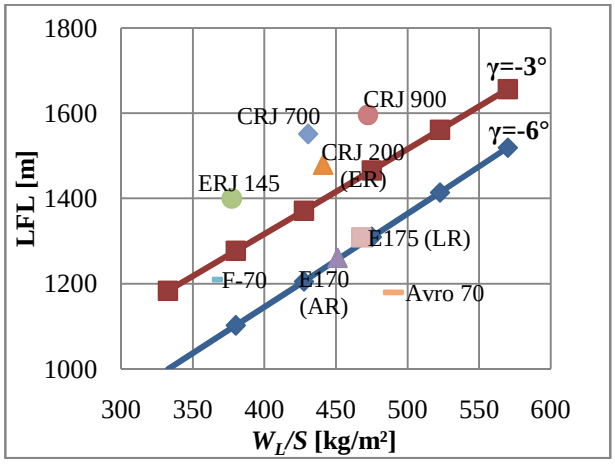

Fig. 14 LFL-method for turbofan compared to aircraft data